Spectral and polarimetric remote sensing for CBRNE applications

Dylan Anderson[1], Leah Appelhans[1], Charles LaCasse[1], Steven Vigil[1], Robert Dzur[2], Trevor Briggs[3], Elizabeth Miller[4], Emily Schultz-Fellenz[4], Julia M. Craven[1]

[1] Sandia National Laboratories, 1515 Eubank Blvd SE, Albuquerque, NM 87123
[2] Bohannan Huston Incorporated, 7500 Jefferson St NE, Albuquerque, NM 87109
[3] Silent Falcon UAS Technologies, 11030 Cochiti Rd SE, Albuquerque, NM 87123
[4] Los Alamos National Laboratory, P.O. Box 1663, Los Alamos, NM 87545

ABSTRACT

Optical remote sensing has become a valuable tool in many application spaces because it can be unobtrusive, search large areas efficiently, and is increasingly accessible through commercially available products and systems. In the application space of chemical, biological, radiological, nuclear, and explosives (CBRNE) sensing, optical remote sensing can be an especially valuable tool because it enables data to be collected from a safe standoff distance. Data products and results from remote sensing collections can be combined with results from other methods to offer an integrated understanding of the nature of activities in an area of interest and may be used to inform in-situ verification techniques. This work will overview several independent research efforts focused on developing and leveraging spectral and polarimetric sensing techniques for CBRNE applications, including system development efforts, field deployment campaigns, and data exploitation and analysis results. While this body of work has primarily focused on the application spaces of chemical and underground nuclear explosion detection and characterization, the developed tools and techniques may have applicability to the broader CBRNE domain.

Keywords: UAS, polarimetry, hyperspectral imaging, underground nuclear explosion, chemical sensing, photogrammetry, remote sensing

1. INTRODUCTION

This paper reviews three recent efforts leveraging spectral and polarimetric sensing for underground nuclear explosion and chemical detection applications. Though each effort is distinct, together they illustrate the diversity of approaches available for applying spectral and polarimetric techniques to the overall chemical, biological, radiological, nuclear, and explosives (CBRNE) sensing domain. Section 2 overviews a remote spectral imagery collection campaign to map a legacy underground nuclear explosion test site. Both spectral imagery and digital elevation model products are produced and are now being used for site analysis and signature exploitation. Section 3 presents on the development of a long wavelength infrared (LWIR) spectropolarimeter for laboratory sample characterization to support radiative transfer model development for remote sensing applications. Finally, section 4 overview a short wavelength infrared (SWIR) tag based polarimetric system for passive and persistent hazardous chemical monitoring and detection. Section 5 presents conclusions and potential future work.

2. UNDERGROUND NUCLEAR EXPLOSION TEST SITE MAPPING AND EXPLOITATION

Currently, detecting, locating, and identifying underground events, such as earthquakes as well as underground conventional and nuclear explosions, is accomplished using networks of sensors recording ground motion (seismometers), or acoustic event signatures (infrasound). The Comprehensive Nuclear Test-ban Treaty Organization's International Monitoring System [1] is one example of such a network. For underground nuclear explosion (UNE) detection specifically, we hypothesize that optical remote sensing data products may assist in clarifying the nature of activities in an area and ultimately confirm or build on the observables obtained by seismic and acoustic techniques.

Chemical, Biological, Radiological, Nuclear, and Explosives (CBRNE) Sensing XX
edited by Jason A. Guicheteau, Chris R. Howle, Proc. of SPIE Vol. 11010, 110100P
 · doi: 10.1117/12.2521098

Declared nuclear test sites provide a unique opportunity to collect against legacy UNE test locations and build a knowledge base of UNE signatures that can manifest as observables in optical remote sensing products. The Nevada National Security Site (NNSS) is a legacy declared nuclear explosion test range in southern Nevada that has been the site of over 800 UNE tests in a variety of different geologies (e.g., tuffs, alluvium, and granite) and emplacement configurations (horizontal tunnels and vertical boreholes). Although the United States entered a moratorium on UNE testing in 1992, the site remains a unique location for characterization of the non-prompt and pervasive signatures that can be produced by nuclear testing. In this work, we performed an extensive collection campaign at a single legacy UNE test site at the NNSS, with the overall strategy that collections over additional sites can be conducted in the future to develop a robust library of observables.

The UNE test location designated as U20az at the NNSS was used as the site of interest in this work. U20az is the site of a vertical borehole emplacement configuration in a thick sequence of volcanic tuff [2]. A 3-D rendering of the area of interest (AOI), including U20az and its surrounds (4.3 km^2) of high desert terrain, is shown in Figure 1. The AOI is bisected by a large canyon and has a 240 m vertical range.

Figure 1. U20az area of interest (4.3 km^2); data shown was collected via manned helicopter in Dec. 2014. Surface ground zero (SGZ) for U20az is labeled with a '*'.

This work focused on collecting high spatial resolution red-green-blue (RGB) imagery, high spectral resolution hyperspectral imagery (HSI), and photogrammetry products over the AOI. Due to the remote, topographically varied nature of the area, an unmanned aerial system (UAS) capable of long range and low altitude flight was used to execute the optical collections. The UAS selected for this work is a class 2 fixed wing solar electric system developed by Silent Falcon UAS Technologies. Two different optical sensors were deployed by UAS to collect the data products of interest. For hyperspectral imagery products, a commercial off the shelf linear pushbroom visible and near infrared (VNIR) hyperspectral imager (HSI, a Headwall Photonics Nano-Hyperspec) with an onboard GPS/IMU was used. This system offers 640 spatial bands and 270 spectral bands over a wavelength range of λ = 400 - 1000 nm. For high spatial resolution imagery and digital elevation products (via photogrammetry), a commercial DSLR camera with a standard Bayer RGB filter (Sony Alpha II) was deployed and integrated with the onboard GNSS navigation system. Due to payload size and weight restrictions imposed by the UAS, each sensor was deployed sequentially.

For geodetic control and reflectance calibration, sixteen ground control points (GCPs) and three reflectance panel calibration targets were installed within the AOI, respectively. Additionally, ground-based point spectra were collected with an ASD Inc. FieldSpec4 Spectroradiometer in and around the AOI to serve as ground truth measurements for the airborne HSI data products. Data collection occurred in June 2016 over 3 days. Although the flight plan called for lines that would include 80% overlap between payload field of view (200 m AGL), high wind conditions during the collection period resulted in some gaps in coverage over the AOI.

The data processing approach taken to convert the raw collected data into imagery mosaic products has been detailed elsewhere [3] [4]. Three principal products were produced. First, the RGB photographs were used to produce an 8-bit RGB orthorectified mosaic with a pixel size of 0.025 meters covering 4.4 km^2, and 72% of the collection AOI, as depicted in Figure 2. The RGB photographs were also used with a photogrammetry software package to produce a digital surface model with 10 cm spatial resolution, as depicted in Figure 3. Finally, 428 hyperspectral images collected over the AOI were georectified and radiometrically calibrated to produce both reflectance and radiance products. An assembled 'quicklook' mosaic of the HSI imagery is depicted in Figure 4.

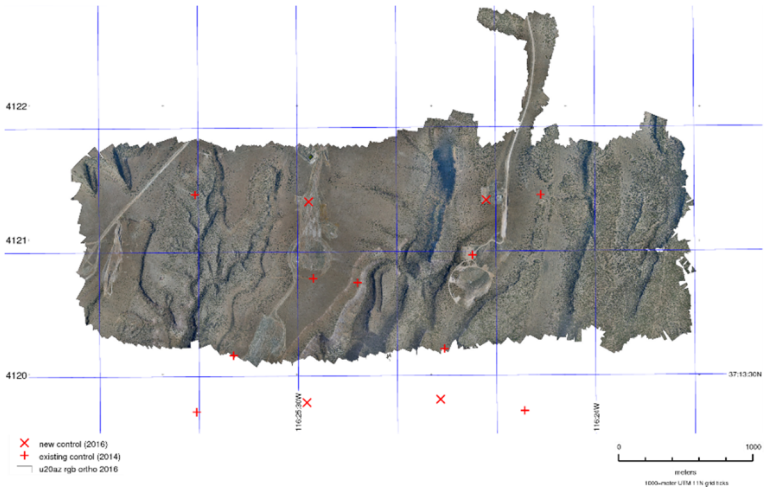

Figure 2. UAS-collected 2.5 cm resolution RGB image mosaic.

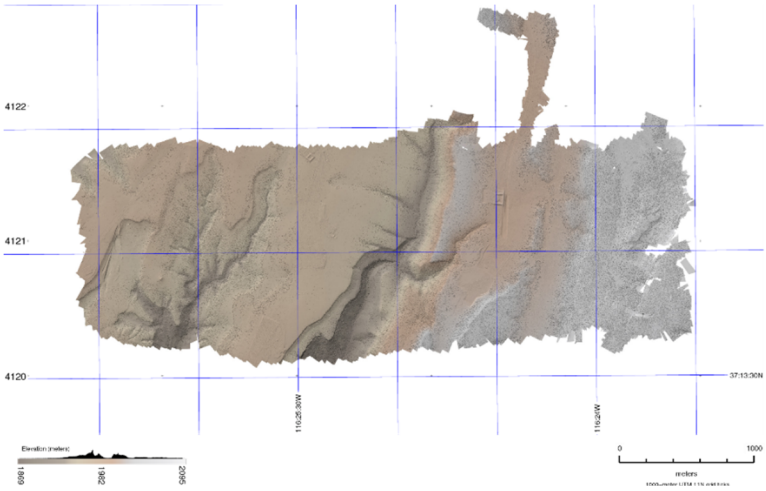

Figure 3. Digital surface model (DSM) of 10 cm resolution elevation data derived photogrammetrically from UAS-collected RGB imagery.

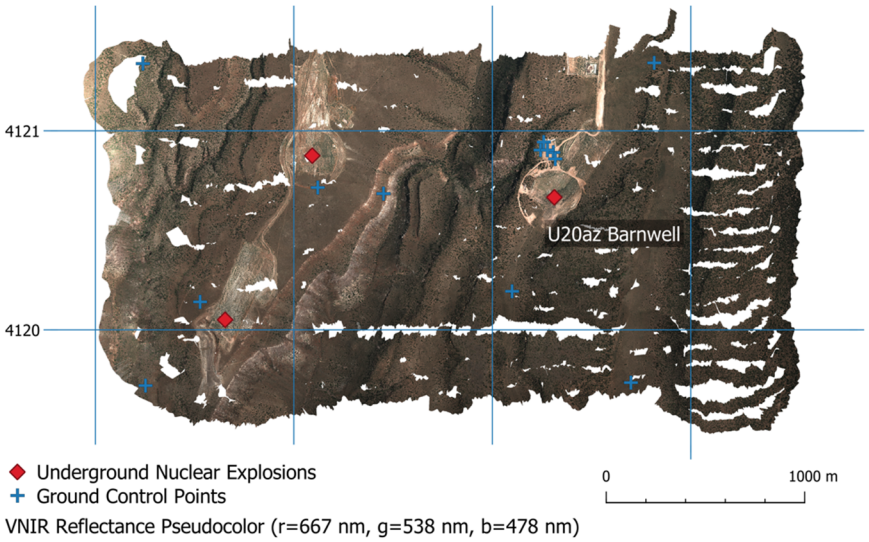

Figure 4. UAS-collected 10 cm resolution VNIR HSI quicklook image mosaic.

The imagery products collected over U20az and its surrounds are being used for ongoing data exploitation and analysis efforts. For example, the digital elevation product produced under this work have been compared to a rotor-based LIDAR elevation product for the same area [5], the RGB imagery has been used for automatic imagery segmentation [6], and the HSI imagery has been used for vegetation classification and invasive species detection [7].

3. LWIR BRDF SPECTROPOLARIMETER DEVELOPMENT

Sophisticated radiative transfer models are being developed to predict the optical reflectance and emission spectra for complex chemical forms such as powders, composites, and dispersed particles [8]. The observed spectra for these materials depend on both the intrinsic (complex index of refraction) and extrinsic (surface morphology) material properties. Producing a robust radiative transfer model for these types of materials benefits from both parametric inputs for sample materials as well as an empirical means to validate predictions.

To support radiative transfer model development, an LWIR (λ = 8.0 – 12 μm) spectropolarimetric bidirectional reflectance distribution function (BRDF) laboratory measurement system was designed and realized. BRDF provides the angularly resolved reflectance of a sample as a function of both illumination and observation geometry. By enabling BRDF measurement as a function of wavelength and incident and observed linear polarization, this system can provide a comprehensive optical characterization of a sample.

The laboratory system was designed to meet high level requirements for supporting radiative transfer model development. First, the system was designed to operate in the LWIR spectral regime to match the frequency regime of focus for model development. Second, the materials of interest for modeling included powders, liquids, and films, including asymmetric samples, and consequently the laboratory system needed to be able to measure these types of materials. Furthermore, accurate characterization of these complex material types drove the system architecture toward the spectrally resolved measurements instead of a laser or other high powered but spectrally limited source.

The principal design challenges associated with realizing this system are detailed elsewhere [9] and included ensuring adequate system throughput, minimizing angular occlusions, and accounting for calibration variation. The system was successfully realized using a combination of commercial off the shelf (COTS) components and custom optics. A CAD rendering of the custom optomechanical system for the angularly resolved measurements is depicted in Figure 5 (a), and a labeled photograph of the assembled system is depicted in Figure 5 (b). A Bruker Vertex 70 FTIR served as the source and detector for the completed system, with the custom BRDF assembly interfaced to the Bruker source exit

port. To achieve angularly resolved measurements, a pair of periscopes with custom gold off axis parabolic mirrors (OAPs) were designed and mated to COTS rotation stages, and the sample stage was mounted on an independent rotation stage. Polarization resolved measurements were enabled by installing broadband wire grid linear COTS polarizers in the base of the source and detector periscopes. The design can accommodate full polarization characterization by the installation of quarter wave retarders in addition to the wire grid polarizers.

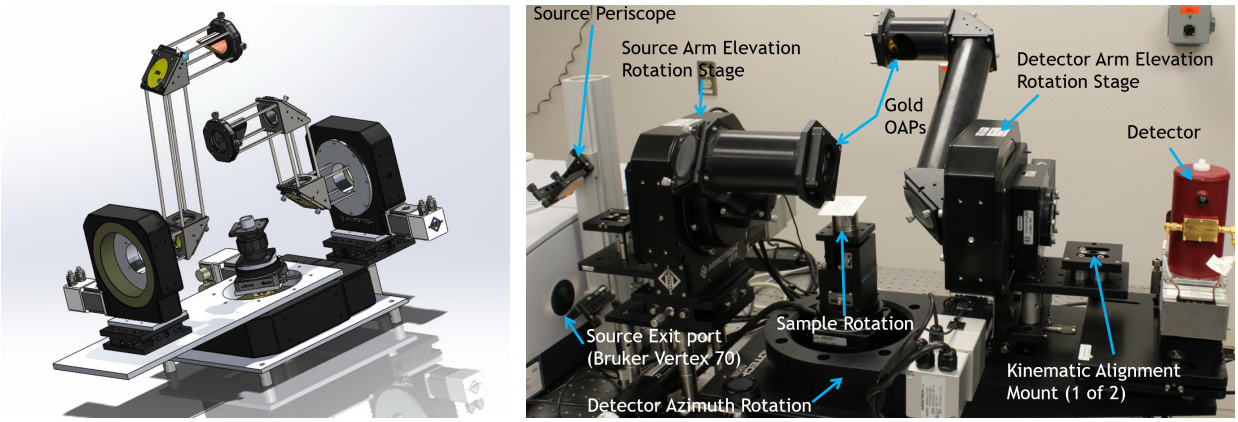

Figure 5. LWIR spectropolarimetric BRDF system. (a) CAD rendering of the custom designed optomechanical assembly and (b) a photograph of the integrated system.

The assembled system is calibrated with a Spectralon Infragold reflectance reference and has been used to measure several different materials. Figure 6 depicts spectropolarimetric reflectance measurement results of a sample of ammonium nitrate powder. These data were collected with a fixed source illumination geometry (-15° elevation), variable detector geometry (0° to 60° elevation in plane), and the four available polarization states (source and receiver *s* or *p* polarized). The specular reflectance lobe is clearly apparent in the data at the 15° detector angle. Additionally, an off specular peak predicted for roughened surfaces in parallel polarization states (*s*-*s* or *p*-*p*) [10] is also observed in the data and absent for crossed polarization states.

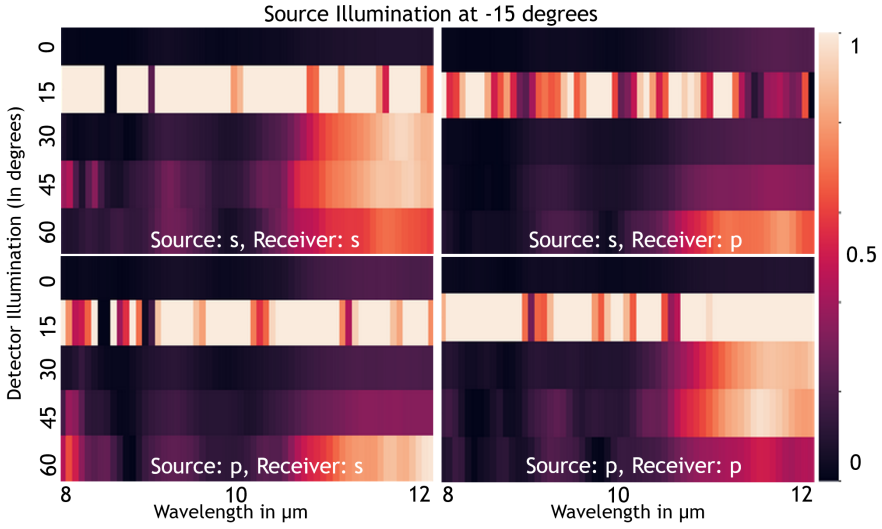

Figure 6. Spectropolarimetric BRDF measurements of ammonium nitrate powder.

4. SWIR POLARIMETRY FOR HAZARDOUS CHEMICAL DETECTION

Techniques for monitoring an area for hazardous chemicals typically rely on either active measurement of material signatures, such as optical absorption or emission features, or total dose accumulation and subsequent chemical analysis. To provide an alternative monitoring approach, a passive polarimetric tag based chemical monitoring system was developed. This system consists of two primary components: a chemically sensitive tag that experiences a permanent change in its polarization properties upon exposure to the chemical of interest, and an imaging polarimeter used to measure the polarization of reflected by the tags (incident from ambient or a low power broadband light source). Both components of the system were developed under this effort. For a proof of concept demonstration, hydrogen fluoride (HF) gas was selected as the chemical of interest and the system was designed to operate in the SWIR (λ = 1.5 – 5.0 µm).

The chemically sensitive tags were produced using a photolithographic process on 4 inch silicon on insulator wafers. Each tag was designed to have a 1 cm square active area, and multiple tags were produced per wafer. The tag design consists of a high frequency periodic structure (nominally a 2.3 µm period with a 50% duty cycle) and an overarching lower frequency 'brick' structure to improve tag robustness. Once etched, the tags were coated with titanium dioxide (TiO2), deposited by a high vacuum electron-beam system, to produce sensitivity to HF gas. Images of the tags at several scales are depicted in Figure 7.

To measure the polarization of light reflected off of the tags, both a laboratory characterization system as well as a portable polarimeter prototype were developed, depicted in Figure 8 (a) and (b) respectively. For both systems, a rotating analyzer measurement approach was implemented to measure the degree of linear polarization (*DOLP*) reflected off of the tags in the SWIR, where

$$DOLP = \frac{\sqrt{S_1^2 + S_2^2}}{S_0}. \quad (1)$$

In Eq. 1, $S_{i=1,2,3}$ are the Stokes parameters associated with total light flux (S_0) and linear polarization (S_1 and S_2) [11].

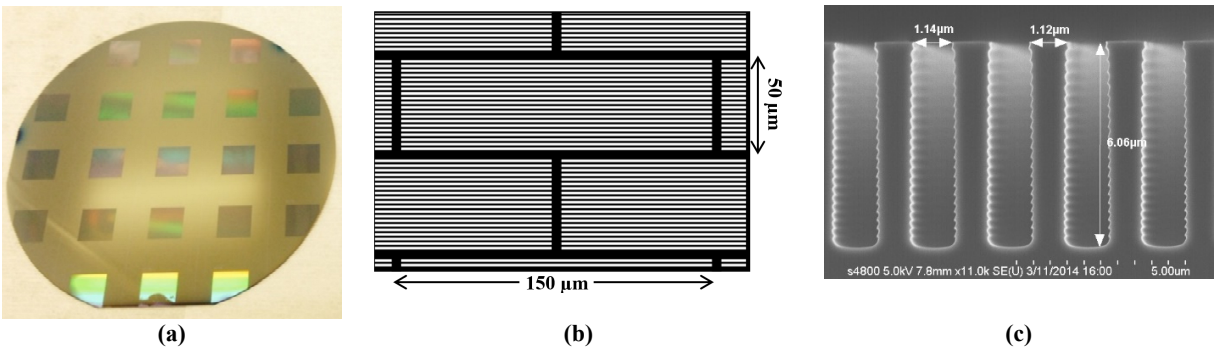

Figure 7. Chemical tag production: (a) one-centimeter tags patterned on a 4 inch wafer, (b) tag subtrate structure, (c) tag cross section.

All results shown here were collected with the laboratory system. A collimated 60 W quartz tungsten halogen (*QTH*) lamp was used as the illumination source. Light reflected from the tag passed through a high extinction ratio analyzing polarizer *A* (Moxtek UBB01A) that rotates to collect the linear polarization measurements, followed by a spectral filter *F* (Spectrogon λ_0 = 2200 nm, $\Delta\lambda \approx$ 100 nm). An InSb camera (FLIR SC6700) with a f/2.5 50 mm effective focal length lens served as the imaging camera. Based on an empirical error analysis for the system [12], spatially averaged *DOLP* value changes of greater than or equal to 0.025 are used to designate the tag has experienced a polarization property change due to HF exposure.

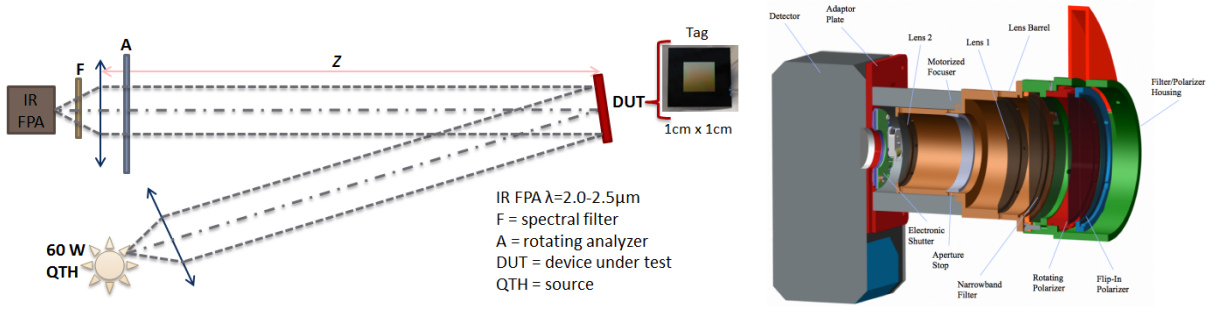

(a) **(b)**

Figure 8: Rotating analyzer polarimeter (a) laboratory testbed system, (b) assembled portable polarimeter.

Tag chemical exposures are performed using a laboratory exposure system based on commercial KIN-TEK permeation sources. HF exposure occurs using a flow of HF with dry nitrogen. Humidity is incorporated using a water bubbler and a static mixer. All exposure tests were performed under RH values ranging from 0% - 45% and HF exposure concentrations from 1 to 40 ppm. Up to eight tags could be exposed in the laboratory system at a time.

Example results (*DOLP* and intensity) for tags exposed to different experimental conditions are depicted in Figure 9. Each row in the figure corresponds to a different tag under test. Intensity data is in arbitrary units. Spatially averaged *DOLP* values for the before and after exposure measurements are used to calculate a total change in *DOLP* ($\Delta DOLP$) experienced by the tag. For all example tags presented in Figure 9, a measurable change in *DOLP* is observed, indicating that chemical detection is possible for these exposure conditions using our tag-based detection system.

To quantify detection limits, Table 1 summarizes the results of all exposure experiments performed. The table is a matrix of exposure conditions with concentrations used corresponding to the columns, and humidity levels corresponding to the rows. Values in the cells represent the total exposure dose (ppm-hours). Finally, color is used to indicate detectability limits; red, yellow, and green indicate that no, some, or all tags exposed to these conditions produced a measurable polarization change, respectively. In general, Table 1 indicates that HF concentrations as low as 1 ppm can be detected, but the presence of water vapor is essential for detection at all tested concentration levels.

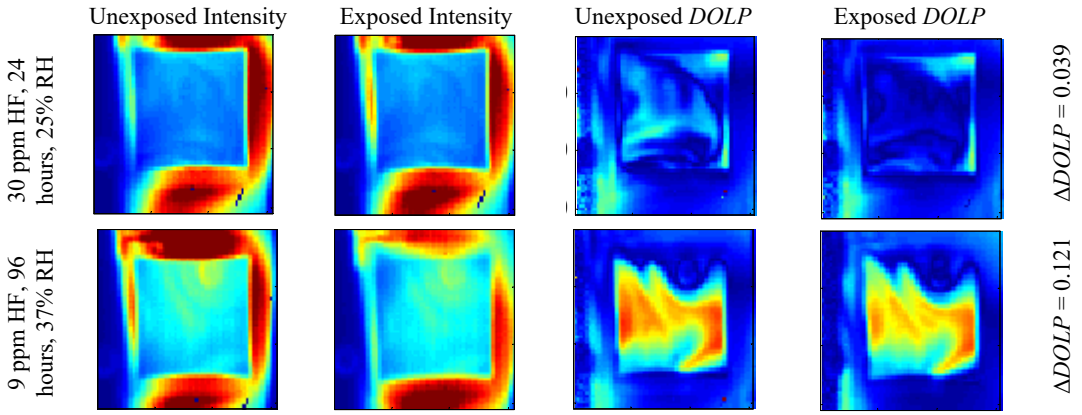

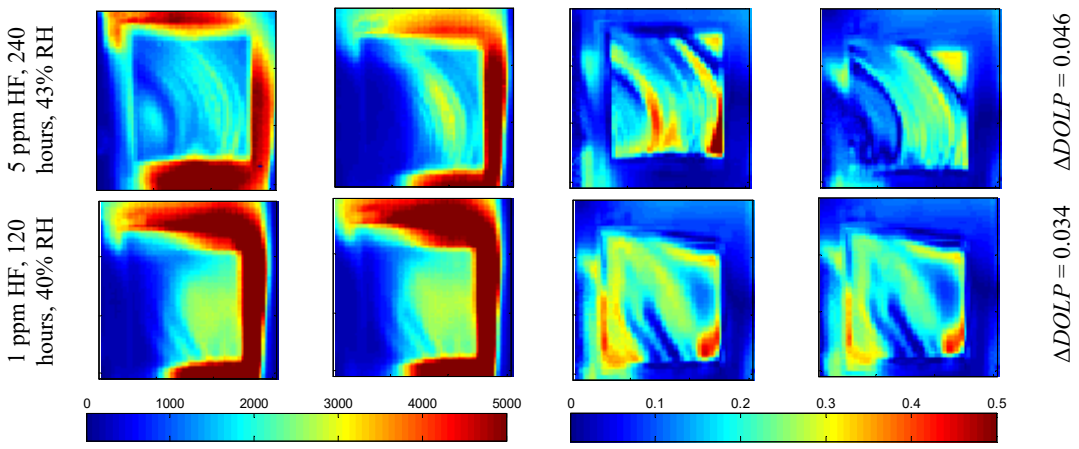

Figure 9. *DOLP* results for prototype tags, measured at λ_0 = 2200 nm and $\Delta\lambda$ = 100 nm.

Table 1. Summary of tag exposure results. Values in the cells represent total exposure dose (ppm-hours).

humidity (%RH) \ HF Concentration (ppm)	1	3	5	7	10	20	30
0	-	-	-	-	-	-	720
10	-	-	-	-	-	-	720, 2880
17-23	720	-	-	-	-	120, 480	720, 1440
28-33	-	406	-	672	-	120, 480	-
35-43	120	-	600, 1200	336, 372	960	120, 480	-

No detectable change | Some detectable change | Consistent detectable change

5. CONCLUSIONS

This paper presented three distinct efforts that apply spectral and polarimetric techniques to CBRNE applications, with a specific focus on underground nuclear explosion and chemical detection. Potential future work for each effort is briefly summarized here. For underground nuclear explosion test site mapping and exploitation, future work should apply the systems and techniques described here to other locations, such as other test site locations at the NNSS, to build on the existing signature and observable knowledge base. Additionally, future UAS mapping campaigns may benefit from the development of alternative HSI architectures that simplify data post-processing. The LWIR spectropolarimetric BRDF system is realized and is being used for material measurements. Future work should include refinement of the calibration methodology to improve system accuracy and efficiency, and additional instrument validation against systems with complimentary measurement capabilities. Finally, for the SWIR chemical detection system, future work should consider building on the existing tag design using alternative detector materials (other than or in addition to TiO_2) to improve sensitivity and environmental robustness.

6. ACKNOWLEDGEMENTS

The authors would like to thank the National Nuclear Security Administration, Defense Nuclear Nonproliferation Research and Development, for sponsoring this work. We would also like to thank the Underground Nuclear

Explosion Signatures Experiment team, a multi-institutional and interdisciplinary group of scientists and engineers, for its technical contributions and support at the NNSS. In particular, we wish to acknowledge the indispensable field support of Michael Floyd, Robert Ziehm, Christian Melchor, and Veraun Chipman; all were with National Security Technologies LLC at the time of our field collections.

Sandia National Laboratories is a multimission laboratory managed and operated by National Technology and Engineering Solutions of Sandia LLC, a wholly owned subsidiary of Honeywell International Inc. for the U.S. Department of Energy's National Nuclear Security Administration under contract DE-NA0003525. SAND2019-5414C. The views expressed in the article do not necessarily represent the views of the U.S. Department of Energy or the United States Government.

7. REFERENCES

[1] "Overview of the verification regime," Preparatory Commission for the Comprehensive Nuclear Test-Ban Treaty Organization, [Online]. Available: https://www.ctbto.org/verification-regime/background/overview-of-the-verification-regime/. [Accessed 13 May 2019].

[2] "United States Nuclear Tests July 1945 through September 1992," U.S. Department of Energy Nevada Operations Office, Las Vegas, 2000.

[3] R. S. Dzur, "Airborne Hyperspectral and Infrared Mapping on the Nevada National Security Site," Bohannan Huston Inc., Albuquerque, 2016.

[4] D. Z. Anderson, J. M. Craven, R. S. Dzur, T. Briggs, D. J. Lee, E. D. Miller, E. S. Schultz-Fellenz and S. Vigil, "Using unmanned aerial systems to collect hyperspectral imagery and digital elevation models at a legacy underground nuclear explosion test site," in *Proceedings of SPIE Vol. 10656*, Orlando, 2018.

[5] S. Vigil, "Airborne and Ground-Based Optical Characterization of Legacy Underground Nuclear Test Sites," in *AGU Fall Meeting*, San Francisco, 2015.

[6] D. J. Lee, D. Anderson and J. Craven, "Integrated Remote Sensing Modalities for Classification at a Legacy Test Site," in *AGU Fall Meeting 2016*, San Francisco, 2016.

[7] B. J. Redman, J. D. van der Laan, D. Z. Anderson, J. M. Craven, E. D. Miller, A. D. Collins, E. M. Swanson and E. S. Schultz-Fellenz, "Hyperspectral vegetation identification at a legacy underground nuclear explosion test site," in *Proceedings of SPIE (In preparation)*, Baltimore, 2019.

[8] T. A. Reichardt and T. J. Kulp, "Radiative transfer modeling of surface chemical deposits," in *Proc. SPIE 9840, Algorithms and Technologies for Multispectral, Hyperspectral, and Ultraspectral Imagery XXII*, Baltimore, 2016.

[9] C. F. LaCasse IV, K. H. Fuerschbach, J. M. Craven, J. W. Segal, J. D. van der Laan, J. B. Wright, S. M. Grover, J. M. Pehr, T. A. Reichardt and T. J. Kulp, "Long wave infrared spectropolarimetric directional reflectometer," in *Proc. SPIE 10655, Polarization: Measurement, Analysis, and Remote Sensing XIII*, Orlando, 2018.

[10] K. E. Torrance and E. M. Sparrow, "Theory for Off-Specular Reflection From Roughened Surfaces," *J. Opt. Soc. Am,* vol. 57, pp. 1105-1114, 1967.

[11] J. S. Tyo, D. L. Goldstein, D. B. Chenault and J. A. Shaw, "Review of passive imaging polarimetry for remote sensing applications," *Appl. Opt.,* vol. 45, pp. 5453-5469, 2006.

[12] J. M. Craven, L. Appelhans, E. J. Couphos, T. Embree, P. S. Finnegan, D. Goldstein, D. Karelitz, C. F. LaCasse, T. S. Luk, A. Mahamat, L. Massey, A. Tanbakuchi, C. Washburn and S. Vigil, "A polarization system for persistent chemical detection," in *Proc. SPIE Vol 9613, Polarization Science and Remote Sensing VII*, San Diego, 2015.